

Supporting Information

Isomers of Pyrene-imidazole Compounds: Synthesis and Configuration Effect on Optical Properties

Yulong Liu,[†] Tong Shan,[†] Liang Yao,[†] Qing Bai,[†] Yachen Guo,[†] Jinyu Li,[†] Xiao Han,[†] Weijun Li,[†] Zhiming Wang,[§] Bing Yang,[†] Ping Lu,^{*,†} and Yuguang Ma[‡]

[†]State Key Laboratory of Supramolecular Structure and Materials, Jilin University, 2699 Qianjin Avenue, Changchun, 130012, China. Email: lup@jlu.edu.cn

[‡]Institute of Polymer Optoelectronic Materials and Devices, State Key Laboratory of Luminescent Materials and Devices, South China University of Technology, Guangzhou, 510640, China

[§]Shenyang University of Technology, Liaoyang, 111003, China

Table of Contents

1. Experimental Section	(2)
2. Synthesis of Materials	(3)
3. Characterization	(5)
3.1 High resolution mass spectrometry (HRMS) spectra of <i>syn</i> -PyDTI and <i>anti</i> -PyDTI.	(5)
3.2 ¹ H NMR spectra of pyrene-4, 5, 9, 10-tetraone and 4-(1, 2, 2-triphenylvinyl) benzaldehyde and ¹ H NMR, ¹³ C NMR spectra of <i>syn</i> -PyDTI and <i>anti</i> -PyDTI.	(6)
3.3 Theoretical calculations of <i>syn</i> -PyDTI and <i>anti</i> -PyDTI.	(10)
3.4 FT-IR spectra of <i>syn</i> -PyDTI and <i>anti</i> -PyDTI.	(12)
3.5 Absorption spectra of <i>syn</i> -PyDTI and <i>anti</i> -PyDTI.	(12)
3.6 Aggregation-induced emission properties for <i>syn</i> -PyDTI and <i>anti</i> -PyDTI.	(13)
3.7 Photographs of <i>syn</i> -PyDTI and <i>anti</i> -PyDTI powder taken under UV illumination.	(14)
3.8 Stacking mode, intermolecular interactions and structure refinements of crystals.	(14)
3.9 Cyclic voltammetry measurement.	(16)
3.10 Thermal analysis: the DSC and TGA graphs of <i>syn</i> -PyDTI and <i>anti</i> -PyDTI.	(16)
3.11 Electroluminescence properties of the devices.	(17)
3.12 Calculation formula for radiative and nonradiative rate constants	(18)

1. Experimental section

All the reagents and solvents used for the syntheses were purchased from Aldrich or Acros companies and used as received. All reactions were performed under a dry nitrogen atmosphere.

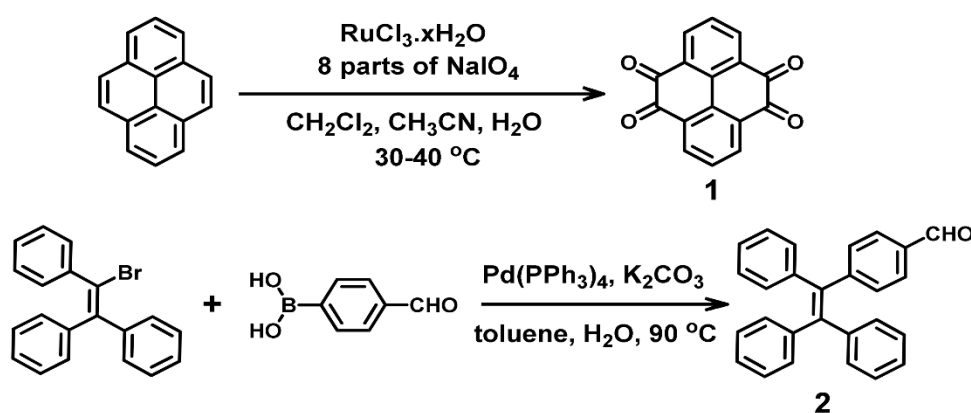
The ^1H NMR and spectra were recorded on AVANCZ 500 spectrometers at 298K by utilizing deuterated dimethyl sulphoxide (DMSO) or tetrahydrofuran (THF) as solvent and tetramethylsilane (TMS) as standard. The final compounds were characterized by Flash EA 1112, CHNS-O elemental analysis instrument, Agilent1290-micrOTOF Q II high resolution mass spectrum analysis instrument. UV-vis absorption spectra were recorded on UV-3100 spectrophotometer for solution and film and recorded on Lambda950 made by PerkinElmer for crystal. Infrared absorption spectrum were recorded on Perkin-Elmer fourier transform infrared spectrometer. Fluorescence measurements were carried out with RF-5301PC. PL efficiencies as well as their fluorescence lifetime in crystalline state and evaporated film were measured using an integrating sphere, with a 366.8 nm Edinburgh Instruments Ltd light emitting diode as the excitation source. Instrument model (FLS920). The differential scanning calorimeter (DSC) analysis was determined using a NETZSCH (DSC-204) instrument at 10 °C/min under nitrogen flushing. Cyclic voltammetry (CV) were performed with a BAS 100W Bioanalytical Systems, using a glass carbon disk ($\Phi = 3$ mm) as working electrode, platinum wire as auxiliary electrode with porous ceramic wick, Ag/Ag^+ as reference electrode, standardized for the redox couple ferricinium/ferrocene. All solutions were purged with nitrogen stream for 10 min before measurement. The procedure was performed at room temperature and nitrogen atmosphere was maintained over the solution during measurements. The ground-state geometries were optimized at the B3LYP/6-31G(d, p) level. The HOMO/LUMO distributions are calculated on the basis of optimized S_0 state.

The single crystals of *syn*-PyDTI and *anti*-PyDTI were prepared by sublimation. Diffraction data were collected on a Rigaku RAXIS-PRID diffractometer using the ω -scan mode with graphite-monochromator $\text{Mo}\cdot\text{K}\alpha$ radiation. The structures were solved with direct methods using SHELXTL and refined with full-matrix least-squares on F^2 .

Device fabrication: The EL devices were fabricated by vacuum deposition of the materials at 10^{-6} Torr onto ITO glass with a sheet resistance of $25 \Omega \text{ square}^{-1}$. All of the organic layers were deposited at a rate of 1.0 \AA s^{-1} . The cathode was deposited with LiF (0.5 nm) at a deposition rate

of 0.1 \AA s^{-1} and then capping with Al metal (120 nm) through thermal evaporation at a rate of 4.0 \AA s^{-1} . The electroluminescent (EL) spectra and Commission Internationale De L'Eclairage (CIE) coordination of these devices were measured by a PR650 spectroscan spectrometer. The luminance-current and density-voltage characteristics were recorded simultaneously with the measurement of the EL spectra by combining the spectrometer with a Keithley model 2400 programmable voltage-current source. All measurements were carried out at room temperature under ambient conditions.

2. Synthesis of Materials



Scheme S1. Synthesis route to monomers.

Synthesis of pyrene-4,5,9,10-tetraone (1):¹ NaIO_4 (35.0 g, 163.6 mmol), H_2O (100.0 mL), and $\text{RuCl}_3 \cdot x\text{H}_2\text{O}$ (0.5 g, 2.4 mmol) were added to a solution of the pyrene (4.0 g, 20 mmol) in CH_2Cl_2 (80.0 mL) and CH_3CN (80.0 mL). The dark brown suspension was heated at $30-40 \text{ }^\circ\text{C}$ overnight. The reaction mixture was extracted by CH_2Cl_2 , the solvent was removed under reduced pressure and then column chromatography (CH_2Cl_2 as the eluent) gave 2.36 g pure products as orange powder. Yield: 45%. $^1\text{H NMR}$ (500 MHz, $\text{C}_2\text{D}_6\text{OS}$, $25 \text{ }^\circ\text{C}$, δ): 8.33 (d, $J = 7.7 \text{ Hz}$, 4H, Ar H), 7.75 (t, $J = 7.8 \text{ Hz}$, 2H, Ar H).

Synthesis of 4-(1,2,2-triphenylvinyl)benzaldehyde (2):² (4-Formylphenyl)boronic acid (0.9 g, 6.0 mmol), (2-bromoethene-1,1,2-triyl)tribenzene (1.7 g, 5.0 mmol), 12 mL of dry toluene, and 9 mL aqueous of Na_2CO_3 solution (2.0 M) were placed in a 50 mL round-bottom flask. $\text{Pd}(\text{PPh}_3)_4$ (104.0 mg, 0.1 mmol) was then added and the mixture was vigorously stirred at $90 \text{ }^\circ\text{C}$ for 48 h. After cooling to room temperature, the resulting mixture was extracted with dichloromethane followed by purification by column chromatography on silica gel with petroleum

ether/dichloromethane (1:1) as the eluent to offer 1.35 g yellow solid. Yield: 75%. ¹H NMR (500 MHz, C₂D₆OS, 25 °C, δ): 9.93 (s, 1H, CH), 7.64 (d, *J* = 8.3 Hz, 2H, Ar H), 7.22 (d, *J* = 8.2 Hz, 2H, Ar H), 7.17–7.11 (m, 10H, Ar H), 7.07–7.02 (m, 5H, Ar H).

Synthesis of PyDTI-based isomers (shown in Scheme 1): A mixture of aniline (4.6 ml, 50.0 mmol), pyrene-4,5,9,10-tetraone (compound 1) (1.3 g, 5.0 mmol), corresponding aromatic aldehyde (TPE-CHO) (compound 2) (4.3 g, 12.0 mmol), ammonium acetate (3.1 g, 40.0 mmol), and acetic acid (20 mL) was refluxed under nitrogen in an oil bath. After 2h, the mixture was cooled and filtered. The solid product was washed with an acetic acid/water mixture (1:1, 150 mL). And then, the two isomers were separated by chromatography using CH₂Cl₂ as eluent and further purified by sublimation under vacuum, giving 1.91 g lightgreen powder (*syn*-PyDTI) and 1.75 g yellow powder (*anti*-PyDTI).

**4,12-diphenyl-5,11-bis(4-(1,2,2-triphenylvinyl)phenyl)-4,12-dihydropyreno[4,5-d:9,10-d']
diimidazole (*syn*-PyDTI)**

Lightgreen powder (yield: 35%). ¹H NMR (500 MHz, C₄D₈O, 25 °C, δ): 9.02 (d, *J* = 7.7 Hz, 2H, Ar H), 8.16 (t, *J* = 7.7 Hz, 1H, Ar H), 7.67–7.58 (m, 10H, Ar H), 7.41 (d, *J* = 8.5 Hz, 4H, Ar H), 7.32 (d, *J* = 8.0 Hz, 2H, Ar H), 7.21 (t, 1H, Ar H), 7.12–7.03 (m, 18H, Ar H), 7.03–6.96 (m, 12H, Ar H), 6.93 (d, *J* = 8.5 Hz, 4H, Ar H); ¹³C NMR (125 MHz, C₄D₈O, 25 °C, δ) 151.3, 144.7, 144.2, 144.1, 143.9, 142.3, 140.9, 139.9, 138.9, 131.74, 131.66, 131.3, 130.5, 130.1, 129.8, 129.6, 129.1, 128.8, 128.1, 128.04, 127.96, 127.4, 127.0, 126.9, 126.8, 126.7, 124.7, 124.0, 119.1, 117.2; IR (KBr): ν = 3381 (w), 3074 (m), 3053 (m), 3024 (m), 1943 (w), 1883 (w), 1804 (w), 1767 (w), 1597 (s), 1500 (s), 1445 (s), 1373 (m), 1324 (m), 1163 (m), 1071 (m), 1029 (m), 853 (m), 798 (m), 750 (s), 721 (s), 697 (s), 627 (m), 584 cm⁻¹ (m); HRMS (ESI) *m/z*: [M + H]⁺ calcd for C₈₂H₅₄N₄, 1095.4421; found, 1095.4383. Anal. calcd for C₈₂H₅₄N₄: C 89.92; H 4.97; N 5.12; found: C 89.88; H 4.79; N 5.34.

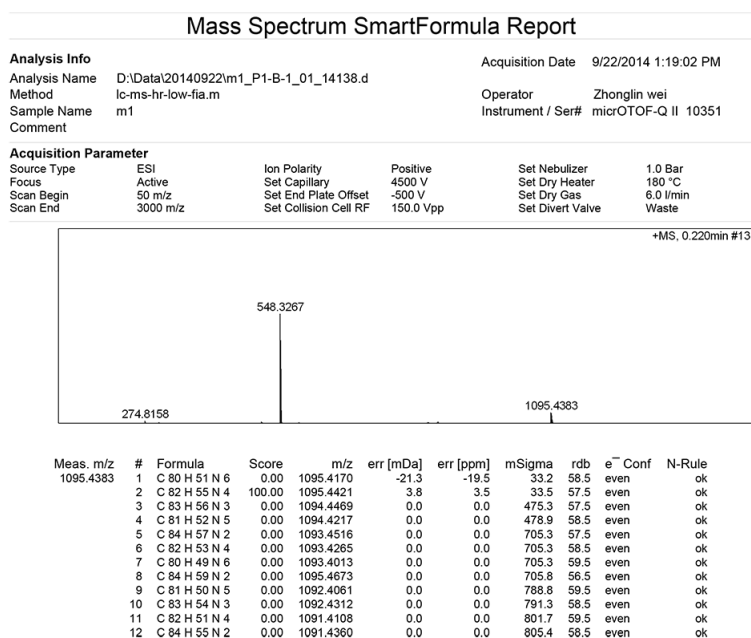
**4,10-diphenyl-5,11-bis(4-(1,2,2-triphenylvinyl)phenyl)-4,10-dihydropyreno[4,5-d:9,10-d']
diimidazole (*anti*-PyDTI)**

Yellow powder (yield: 32%), ¹H NMR (500 MHz, C₄D₈O, 25 °C, δ): 8.91 (d, *J* = 6.6 Hz, 2H, Ar H), 7.74–7.64 (m, 12H, Ar H), 7.45–7.41 (m, 6H, Ar H), 7.12–7.03 (m, 18H, Ar H), 7.03–6.97 (m,

12H, Ar H), 6.93 (d, $J = 8.5$ Hz, 4H, Ar H); ^{13}C NMR (125 MHz, CDCl_3 , 25 °C, δ) 131.84, 131.81, 131.4, 131.3, 131.18, 131.15, 128.6, 128.0, 127.9, 127.7, 126.9; IR (KBr): $\nu = 3075$ (m), 3048 (m), 3020 (m), 1936 (w), 1878 (w), 1801 (w), 1784 (w), 1758 (w), 1595 (s), 1497 (s), 1463 (s), 1444 (s), 1408 (m), 1375 (s), 1323 (m), 1174 (m), 1073 (m), 858 (s), 797 (s), 772 (s), 751 (s), 717 (s), 695 (s), 655 (s), 627 cm^{-1} (s); HRMS (ESI) m/z : $[\text{M} + \text{H}]^+$ calcd for $\text{C}_{82}\text{H}_{54}\text{N}_4$, 1095.4421; found, 1095.4357. Anal. calcd for $\text{C}_{82}\text{H}_{54}\text{N}_4$: C 89.92; H 4.97; N 5.12; found: C 89.74; H 5.06; N 5.21.

3. Characterization

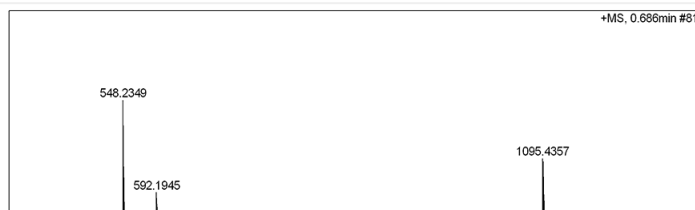
3.1 High resolution mass spectrometry (HRMS) spectra of *syn*-PyDTI and *anti*-PyDTI



Mass Spectrum SmartFormula Report

Analysis Info		Acquisition Date	9/22/2014 1:47:41 PM	
Analysis Name	D:\Data\20140922\m2_P1-B-5_01_14144.d	Operator	Zhonglin wei	
Method	lc-ms-hr-wide-fia.m	Instrument / Ser#	micrOTOF-Q II 10351	
Sample Name	m2	Comment		

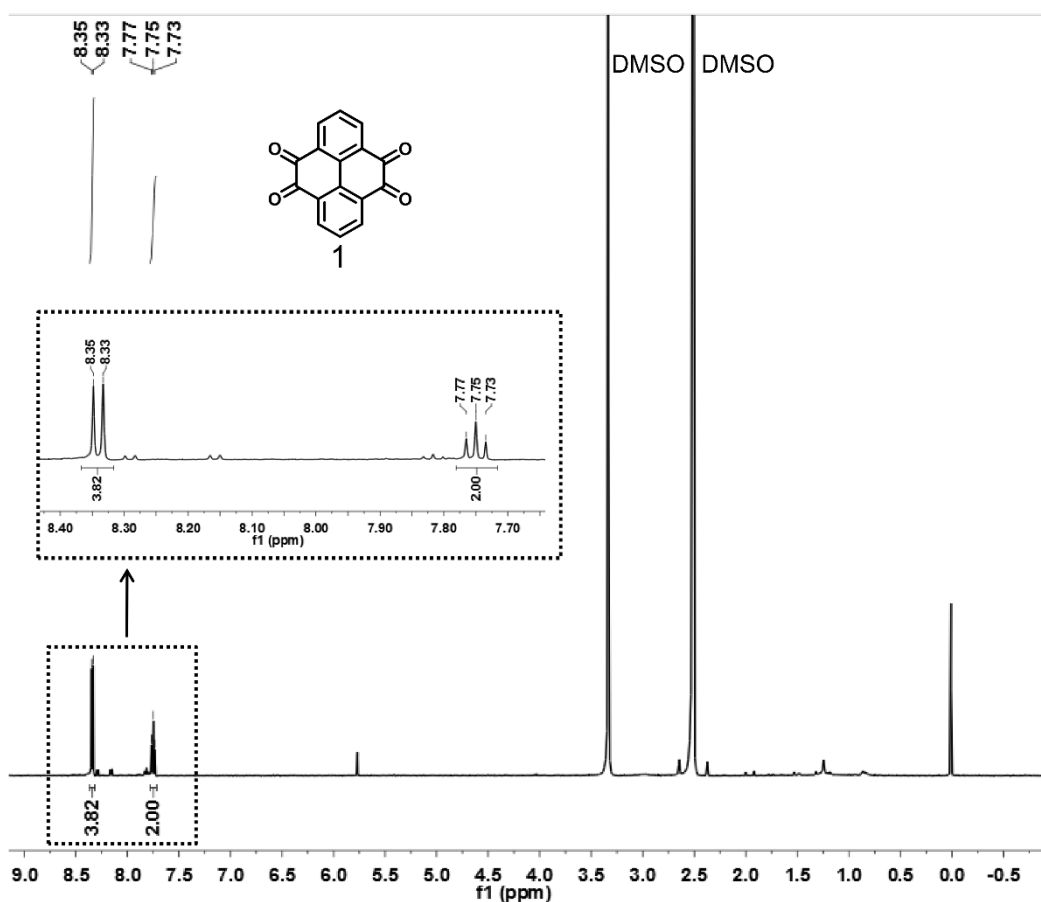
Acquisition Parameter					
Source Type	ESI	Ion Polarity	Positive	Set Nebulizer	1.0 Bar
Focus	Active	Set Capillary	4500 V	Set Dry Heater	200 °C
Scan Begin	50 m/z	Set End Plate Offset	-500 V	Set Dry Gas	6.0 l/min
Scan End	3000 m/z	Set Collision Cell RF	600.0 Vpp	Set Divert Valve	Waste



Meas. m/z	#	Formula	Score	m/z	err [mDa]	err [ppm]	mSigma	rdb	e ⁻ Conf	N-Rule
1095.4357	1	C 80 H 51 N 6	0.00	1095.4170	-18.7	-17.1	28.7	58.5	even	ok
	2	C 82 H 55 N 4	100.00	1095.4421	6.4	5.9	29.0	57.5	even	ok
	3	C 75 H 55 N 10	0.00	1095.4606	24.9	22.7	42.1	53.5	even	ok
	4	C 75 H 180 N	0.00	1095.4110	-24.7	-22.5	50.6	-13.5	even	ok
	5	C 83 H 56 N 3	0.00	1094.4469	0.0	0.0	474.6	57.5	even	ok
	6	C 81 H 52 N 5	0.00	1094.4217	0.0	0.0	478.1	58.5	even	ok
	7	C 74 H 52 N 11	0.00	1094.4402	0.0	0.0	538.5	54.5	even	ok
	8	C 76 H 181	0.00	1094.4158	0.0	0.0	539.5	-13.5	even	ok
	9	C 84 H 59 N 2	0.00	1095.4673	0.0	0.0	682.2	56.5	even	ok
	10	C 80 H 49 N 6	0.00	1093.4013	0.0	0.0	702.1	59.5	even	ok

Figure S1. High resolution mass spectrometry (HRMS) spectra of *syn*-PyDTI (up) and *anti*-PyDTI (down).

3.2 ¹H NMR spectra of pyrene-4,5,9,10-tetraone (1) and 4-(1,2,2-triphenylvinyl) benzaldehyde (2) and ¹H NMR, ¹³C NMR spectra of *syn*-PyDTI and *anti*-PyDTI.



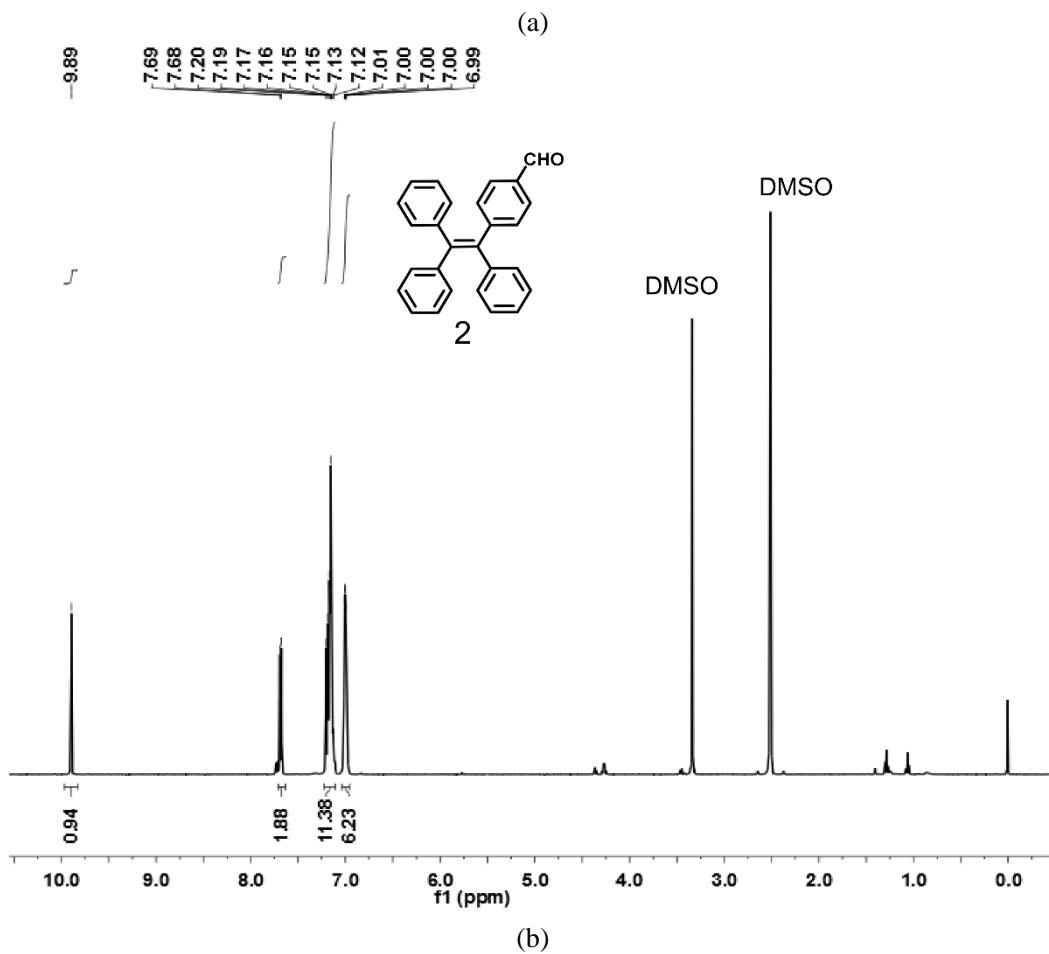
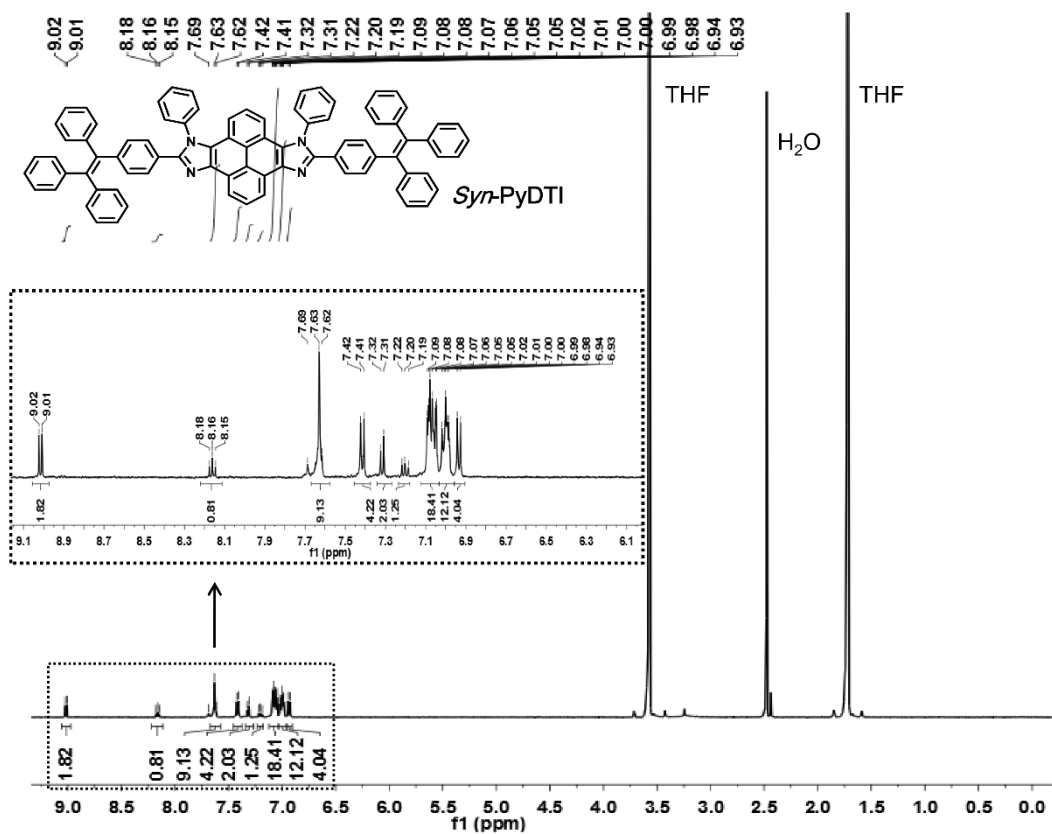
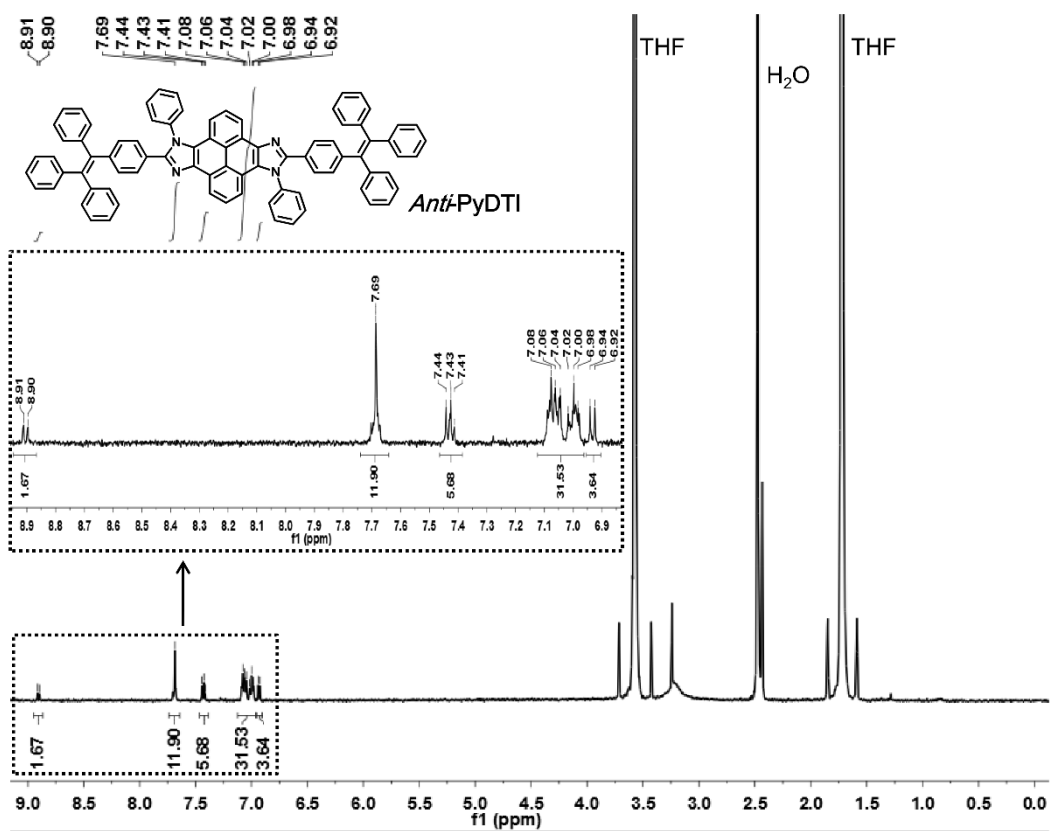


Figure S2. ^1H NMR (500 MHz) spectra of pyrene-4,5,9,10-tetraone (a) and 4-(1,2,2-triphenylvinyl) benzaldehyde (b) measured in $\text{C}_2\text{D}_6\text{OS}$.

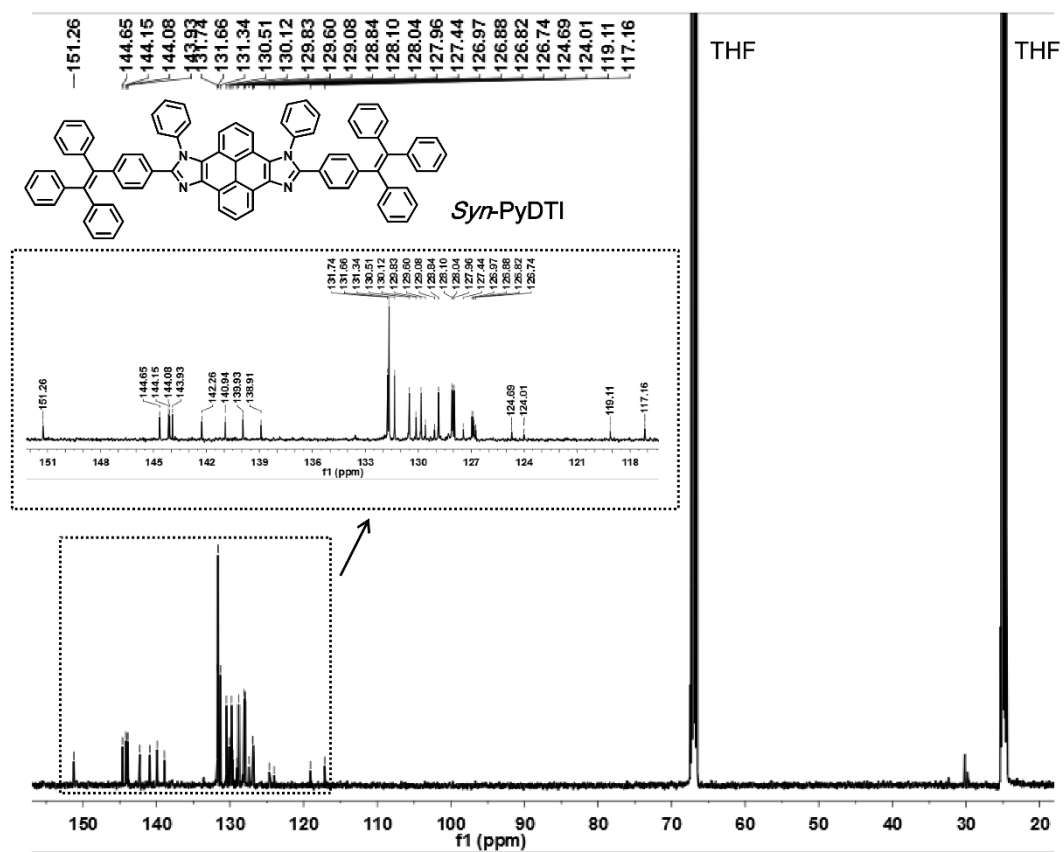


(a)



(b)

Figure S3. ¹H NMR (500 MHz) spectra of *syn*-PyDTI (a) and *anti*-PyDTI (b) measured in C₄D₈O.



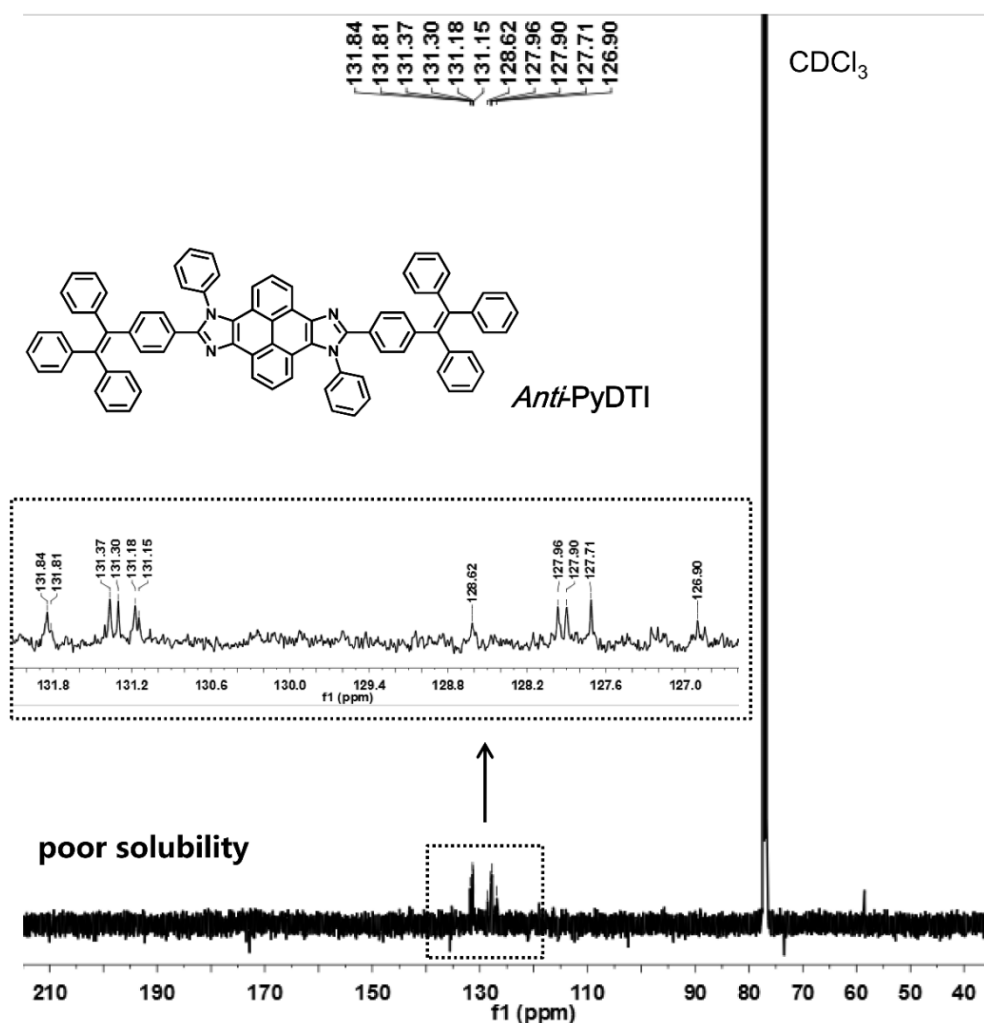


Figure S5. ¹³C NMR (125 MHz) spectra of *anti*-PyDTI measured in CDCl₃.

3.3 Theoretical calculations of *syn*-PyDTI and *anti*-PyDTI

3.3.1 HOMO and LUMO distributions of *syn*-PyDTI and *anti*-PyDTI

The distribution of the highest occupied molecular orbitals (HOMOs) were very similar for *syn*-PyDTI and *anti*-PyDTI which were mainly located on pyrene-imidazole segment. The lowest unoccupied molecular orbitals (LUMOs) of *anti*-PyDTI were delocalized over the whole molecule, while LUMOs of *syn*-PyDTI were delocalized mainly on TPE group with sizable distribution on upper part of pyrene which probably resulted from the distinct dipole orientation in *syn*-PyDTI.

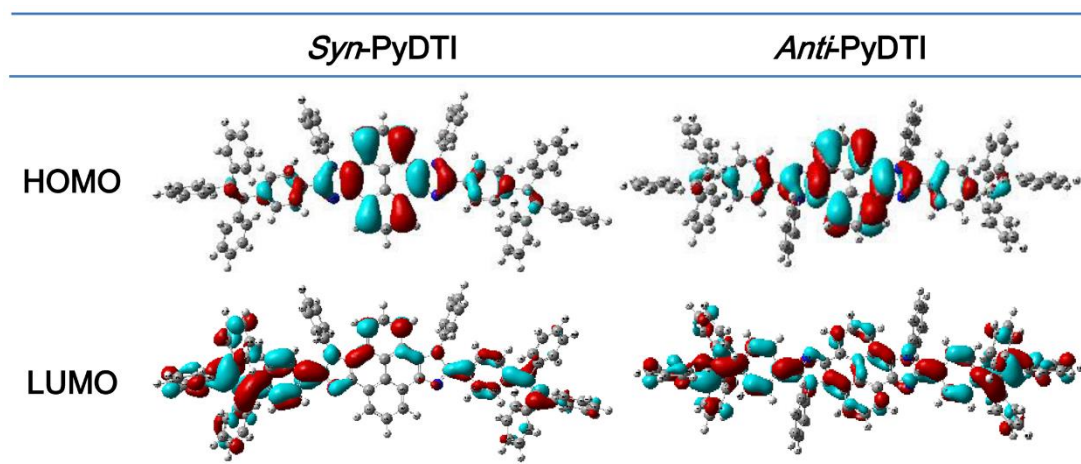


Figure S6. HOMO and LUMO distributions of *syn*-PyDTI and *anti*-PyDTI on the basis of DFT results at the B3LYP/6-31G(d, p) level.

3.3.2 Optimization of molecular configuration and the direction of dipole in ground state

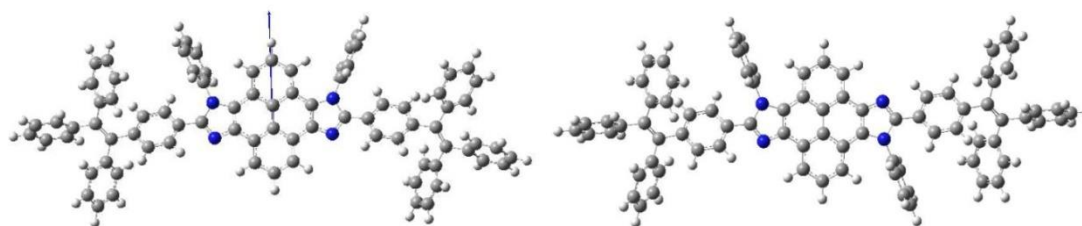


Figure S7. Optimization of molecular configuration and the direction of dipole in ground state on the basis of DFT results at the B3LYP/6-31G(d,p) level.

Table S1. The calculated total energy and ground state, excited state dipole moments based on B3LYP/6-311G (d,p) level.

<i>syn</i> -PyDTI	Energy (eV)	x	y	z	D
Ground state	-91877.288	-0.3584	-6.5056	1.2385	6.6322
Excited state	-91840.082	-0.3815	-6.6901	1.2344	6.8183
<i>anti</i> -PyDTI	Energy (eV)	x	y	z	D
Ground state	-91877.319	-0.0004	0.0000	0.0008	0.0009
Excited state	-91836.509	-0.0003	0.0000	0.0009	0.0009

3.4 FT-IR spectra of *syn*-PyDTI and *anti*-PyDTI

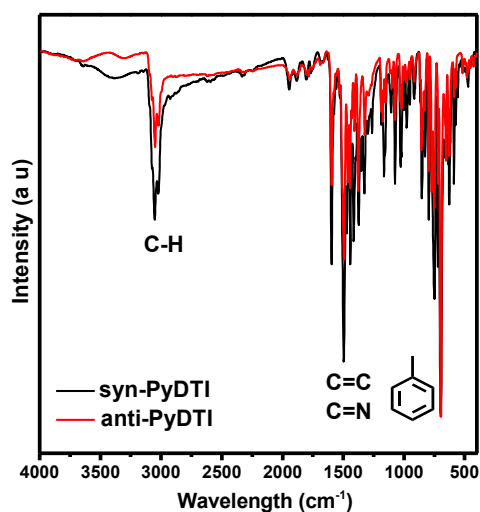


Figure S8. FTIR spectra of *syn*-PyDTI and *anti*-PyDTI under same condition (Scan range: 400–4000 cm^{-1}).

3.5 Absorption spectra of *syn*-PyDTI and *anti*-PyDTI

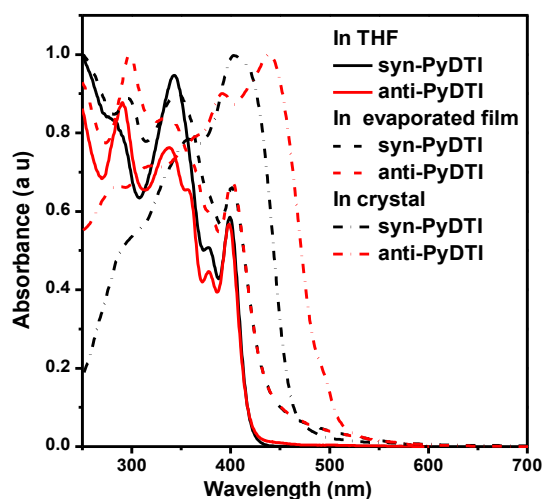


Figure S9. Normalized absorption spectra of *syn*-PyDTI and *anti*-PyDTI in tetrahydrofuran (THF), evaporated film and crystal. Concentration in THF: $1 \times 10^{-5} \text{ mol L}^{-1}$; Film thickness: 30 nm.

Employing the absorption spectrum of *syn*-PyDTI in dilute THF as a representative, the absorption peaks at 276 nm and 343 nm were originated from pyrene group, and the peaks in the longer-wavelength region of 377 and 398 nm were ascribed to pyreneimidazole-localized π - π^* electronic excitation. The absorption spectra for each isomers in amorphous evaporated film were very similar to that of solution, except that the absorption edges were red-shifted about 10 nm with less vibrational fine structure.

Table S2. Optical and Electrochemical Properties of *syn*-PyDTI and *anti*-PyDTI.

Isomer	UV(solu) ^a (nm)	UV(film) ^b (nm)	UV(cry) ^c (nm)	PL(film) ^b (nm)	PL(cry) (nm)	E _g ^d (eV)	E _g ^e (eV)
<i>syn</i> -PyDTI	276,343,377,399	295,345,400	305,358,403	495	465	2.83	2.77
<i>anti</i> -PyDTI	289,338,357,378, 398	297,335,362, 400	280,318,390, 438	495	485,507, 530	2.83	2.85

^aMeasured in dilute tetrahydrofuran solution (concentration: 1×10^{-5} mol L⁻¹). ^bmeasured in evaporated film (30nm). ^cMeasured through photoreflectance method based on barium sulfate. ^dEstimated by the absorption on set values in film. ^eEstimated by Cyclic voltammogram.

3.6 Aggregation-induced emission properties of *syn*-PyDTI and *anti*-PyDTI

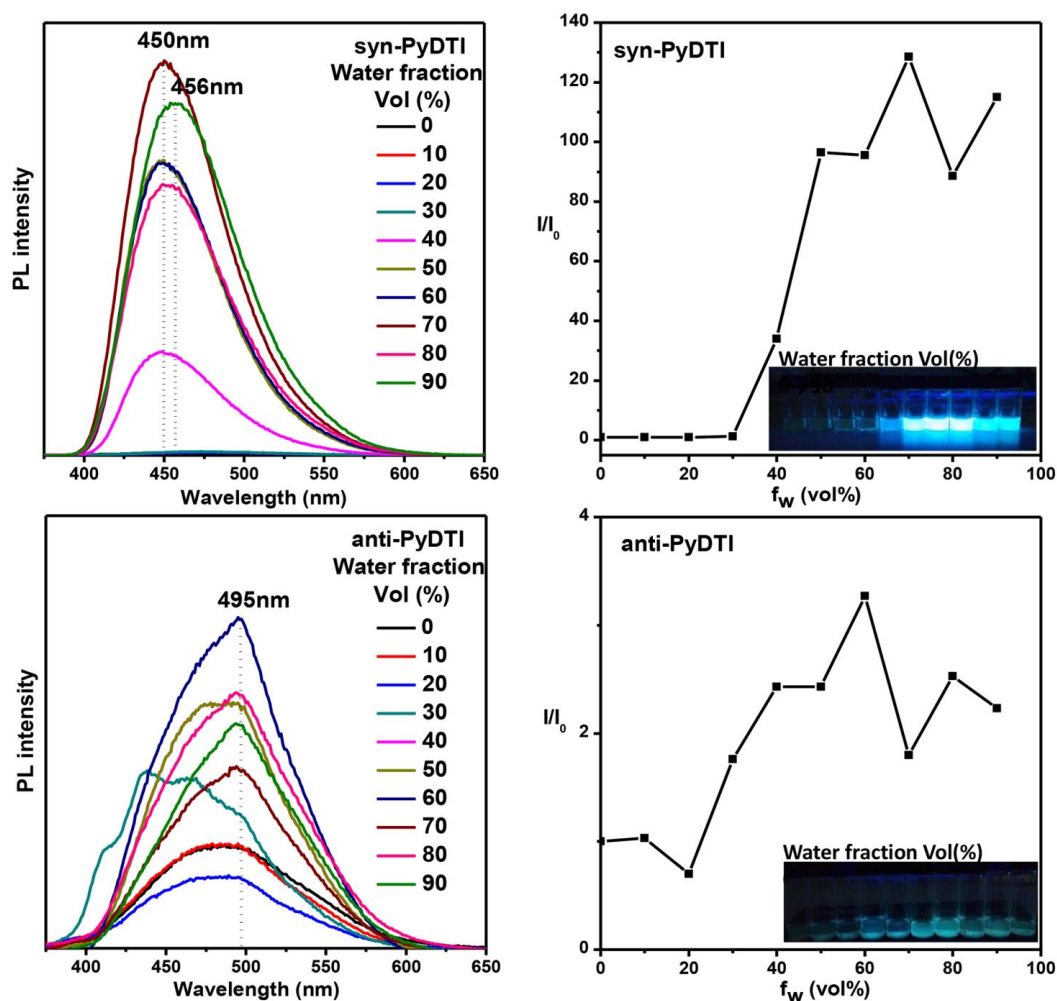


Figure S10. Left: PL spectra of *syn*-PyDTI and *anti*-PyDTI in THF/water mixtures with different water fractions (f_w). Right: Plots of (I/I_0) values as a function of f_w in THF/water mixtures of *syn*-PyDTI and *anti*-PyDTI, in which I_0 is the PL intensity in pure THF solution.

3.7 Photographs of *syn*-PyDTI and *anti*-PyDTI powder taken under UV illumination

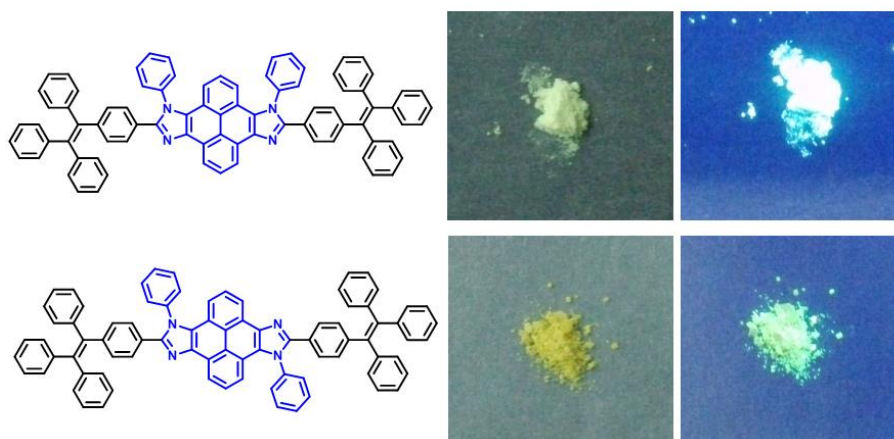


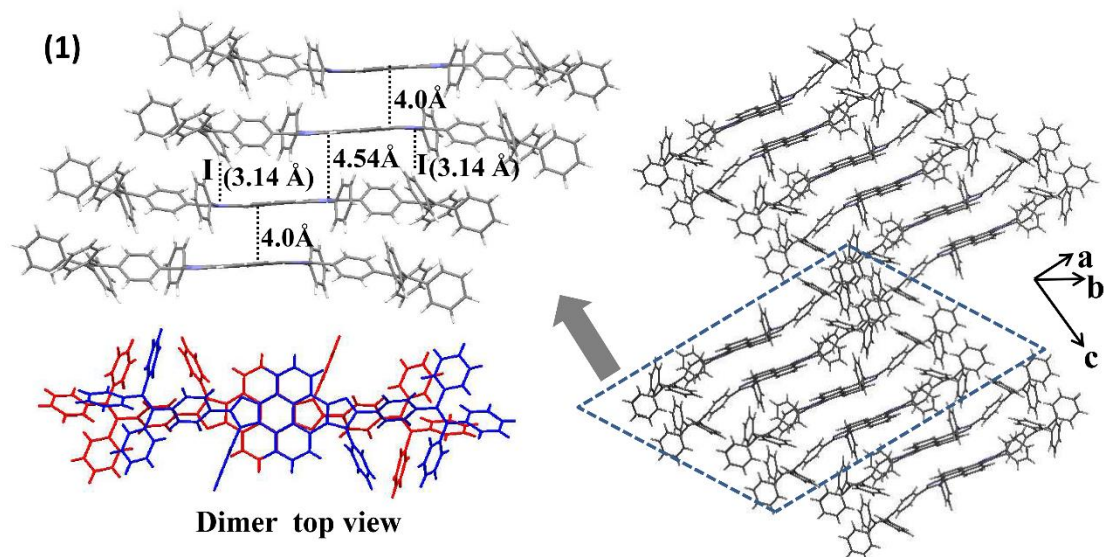
Figure S11. Photographs of *syn*-PyDTI and *anti*-PyDTI powder taken under UV illumination.

3.8 Stacking mode and crystal data and structure refinements of crystals

CCDC 1406607 and 1406608 contain the supplementary crystallographic data for this paper. These data can be obtained free of charge from The Cambridge Crystallographic Data Centre via www.ccdc.cam.ac.uk/data_request/cif.

Syn-PyDTI: The distance between neighbouring dimers was also relatively big as ~ 4.54 Å. Careful analysis of the data found that only one C-H $\cdots\pi$ interaction (I) existed between the hydrogen atom of TPE and the π -electrons of imidazole with a distance of 3.14 Å.

Anti-PyDTI: There were four C-H $\cdots\pi$ (II, III, IV, V) interactions between hydrogen atom on phenyl rings of TPE and the π clouds of the aromatic ring of pyrene-imidazole in adjacent molecules with distances of 2.74-2.90 Å, and one C-H $\cdots\pi$ (I) interaction between hydrogen atom on phenyl ring attaching to the N atom of imidazole and phenyl ring connecting with imidazole in TPE with a distance of 2.96 Å.



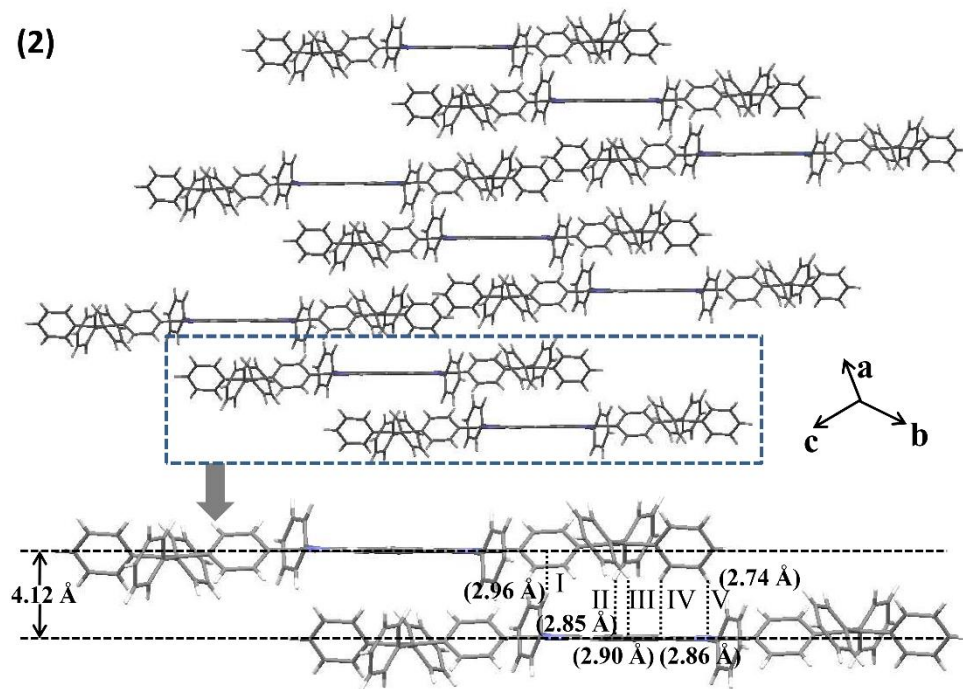


Figure S12. Stacking image and intermolecular interactions of *syn*-PyDTI (1) and *anti*-PyDTI (2).

Table S3. Crystal data and structure refinements of crystals

	<i>syn</i> -PyDTI	<i>anti</i> -PyDTI
empirical formula	C ₈₂ H ₅₄ N ₄	C ₈₂ H ₅₄ N ₄
formula wt	1095.29	1095.29
<i>T</i> , K	296(2)	296(2)
crystal system	Triclinic	Triclinic
space group	P -1	P -1
<i>a</i> , Å	10.0347(8)	10.1789(4)
<i>b</i> , Å	11.9855(10)	11.9937(5)
<i>c</i> , Å	25.329(2)	13.2135(5)
α ,deg	77.339(2)	108.6000(10)
β ,deg	87.855(2)	95.1890(10)
γ ,deg	87.767(2)	102.3540(10)
<i>V</i> ,Å ³	2968.7(4)	1471.38(10)
<i>Z</i>	2	1
density, Mg/m ³	1.225	1.236
Absorption coefficient, mm ⁻¹	0.071	0.072
θ range, deg	0.82-24.66	1.65-28.80
no. of reflns collected	18563	12741
no. of unique reflns	9994	7563
<i>R</i> (int)	0.0486	0.0163
Good-of-fit on F ²	1.019	1.018
<i>R</i> 1 [<i>I</i> > 2 σ (<i>I</i>)]	0.0527	0.0480
<i>wR</i> 2 [<i>I</i> > 2 σ (<i>I</i>)]	0.1406	0.1244
<i>R</i> 1 (all data)	0.0835	0.0723
<i>wR</i> 2 (all data)	0.1671	0.1416

3.9 Cyclic voltammetry measurement of *syn*-PyDTI and *anti*-PyDTI

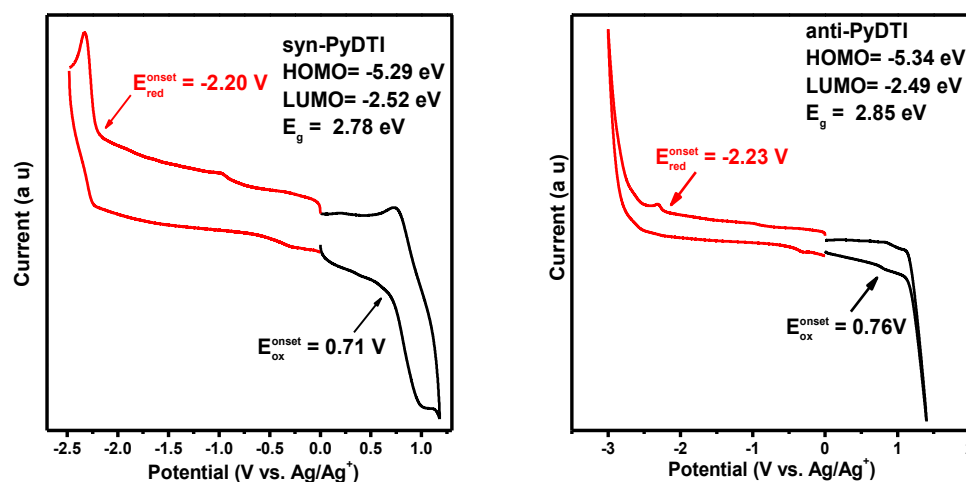


Figure S13. Cyclic voltammogram of *syn*-PyDTI and *anti*-PyDTI in CH_2Cl_2 (oxidation) and DMF (reduction), measured with 0.1 M $(\text{Bu}_4\text{N})\text{PF}_6$ as supporting electrolyte at a scan rate of 100 mV s^{-1} .

The *syn*- and *anti*-isomers shared the very similar CV behaviors. Both of them underwent irreversible oxidation and reduction process as estimated by cyclic voltammetry in 0.1 M solution of $(\text{Bu}_4\text{N})\text{PF}_6$ in dry dichloromethane under Ar atmosphere. According to the onset potentials, the highest occupied molecular orbital (HOMO) levels of *syn*-PyDTI and *anti*-PyDTI were calculated to be -5.29 and -5.34 eV, while the lowest unoccupied molecular orbital (LUMO) levels of *syn*-PyDTI and *anti*-PyDTI were calculated to be -2.52 eV and -2.49 eV, respectively, by comparison to ferrocene. The HOMO-LUMO energy gaps obtained from CV measurement coincided well with the optical energy gaps got from UV-vis measurements (Table S2).

3.10 Thermal Analysis: The DSC and TGA graphs of *syn*-PyDTI and *anti*-PyDTI

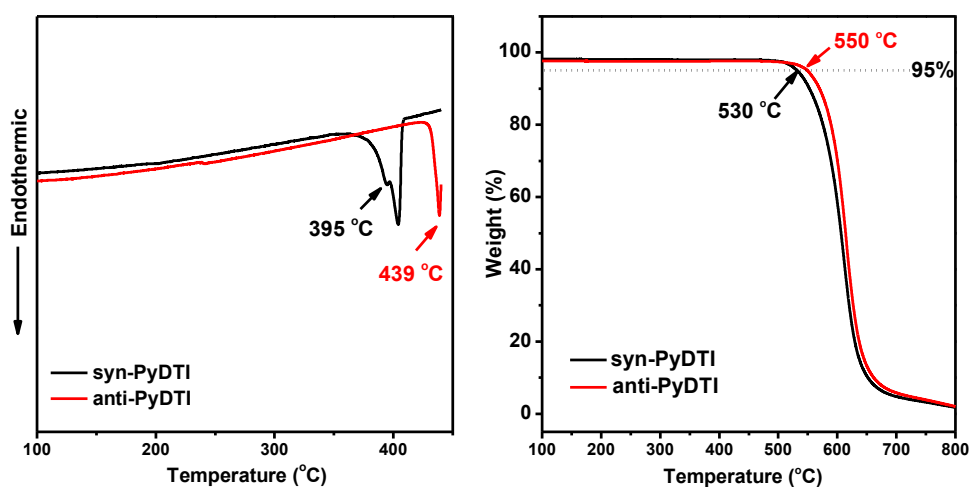


Figure S14. DSC and TGA thermograms of *syn*-PyDTI and *anti*-PyDTI under nitrogen at a heating rate of $10 \text{ }^\circ\text{C min}^{-1}$.

Syn-PyDTI and *anti*-PyDTI exhibited excellent thermal stability with decomposition temperature (5% weight loss) at 530 °C and 550 °C, respectively. In DSC heating cycles, no T_g was detected for both isomers due to their rigid polycyclic skeleton, and T_m appeared at 395 °C and 439 °C for *syn*-PyDTI and *anti*-PyDTI, respectively, demonstrating their high thermostability. The comparatively lower T_d and T_m of *syn*-PyDTI might be caused by the more flexible molecular feature by the axisymmetric characteristic as observed from the crystal structure.

3.11 Electroluminescence performance of *syn*-PyDTI and *anti*-PyDTI

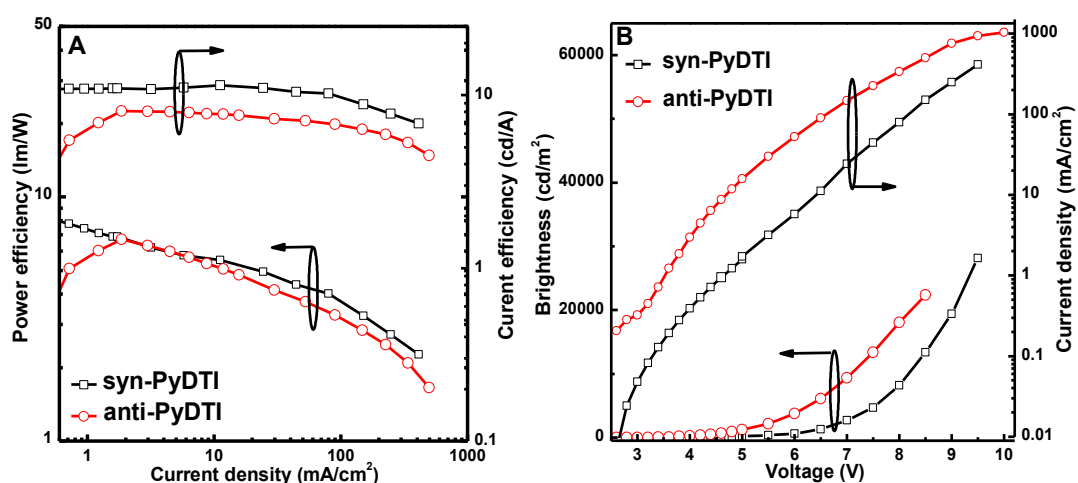


Figure S15. a) Current efficiency and power efficiency versus current density curves. b) Current density–voltage–brightness (J–V–L) characteristics.

Table S4. Electroluminescence properties of the devices

Isomer Device	V_{on} (V) ^a	LE (cd A ⁻¹) ^b			EQE (%) ^c	Brightness (cd m ⁻²)	EL (nm)
		Max	@1000 cd m ⁻²	@10000 cd m ⁻²			
<i>syn</i> -PyDTI	2.8	11.42	11.33	9.62	4.41	28150	500
<i>anti</i> -PyDTI	2.8	8.12	7.75	6.30	3.0	22359	508

^a Turn-on voltage at which emission became detectable. ^b current efficiency. ^c External quantum efficiency.

3.12 Calculation formula for Radiative and nonradiative rate constants

Radiative (k_r) and nonradiative (k_{nr}) rate constants can be calculated by applying the equations S1 -S4,¹ where Φ is the fluorescence quantum yield and τ is the fluorescence lifetime. In the case of multiexponential decay, the weighted average of the fluorescence lifetime values was used for the estimation of rates of radiative and nonradiative processes (Table 1).

$$\Phi = \frac{k_r}{k_r + k_{nr}} \quad (1)$$

$$\tau = \frac{1}{k_r + k_{nr}} \quad (2)$$

$$k_r = \frac{\Phi}{\tau} \quad (3)$$

$$k_{nr} = \frac{1}{\tau} - k_r \quad (4)$$

References

1. Hu, J.; Zhang, D.; Harris, F. W. *J. Org. Chem.* **2005**, *70*, 707.
2. Hu, R. R.; Maldonado, J. L.; Rodriguez, M.; Deng, C. M.; Jim, C. K. W.; Lam, J. W. Y.; Yuen, M. M. F.; Ortiz, G. R.; Tang, B. Z. *J. Mater. Chem.* **2012**, *22*, 232.
3. J. R. Lakowicz, *Principles of Fluorescence Spectroscopy*, Plenum Press, New York, USA, 1999.